CHEMISTRY
A EUROPEAN JOURNAL

DOI: 10.1002/chem.200903582

Steric and Electronic Influence on Photochromic Switching of N,C-Chelate Four-Coordinate Organoboron Compounds

Hazem Amarne, Chul Baik, Stephen K. Murphy, and Suning Wang*[a]

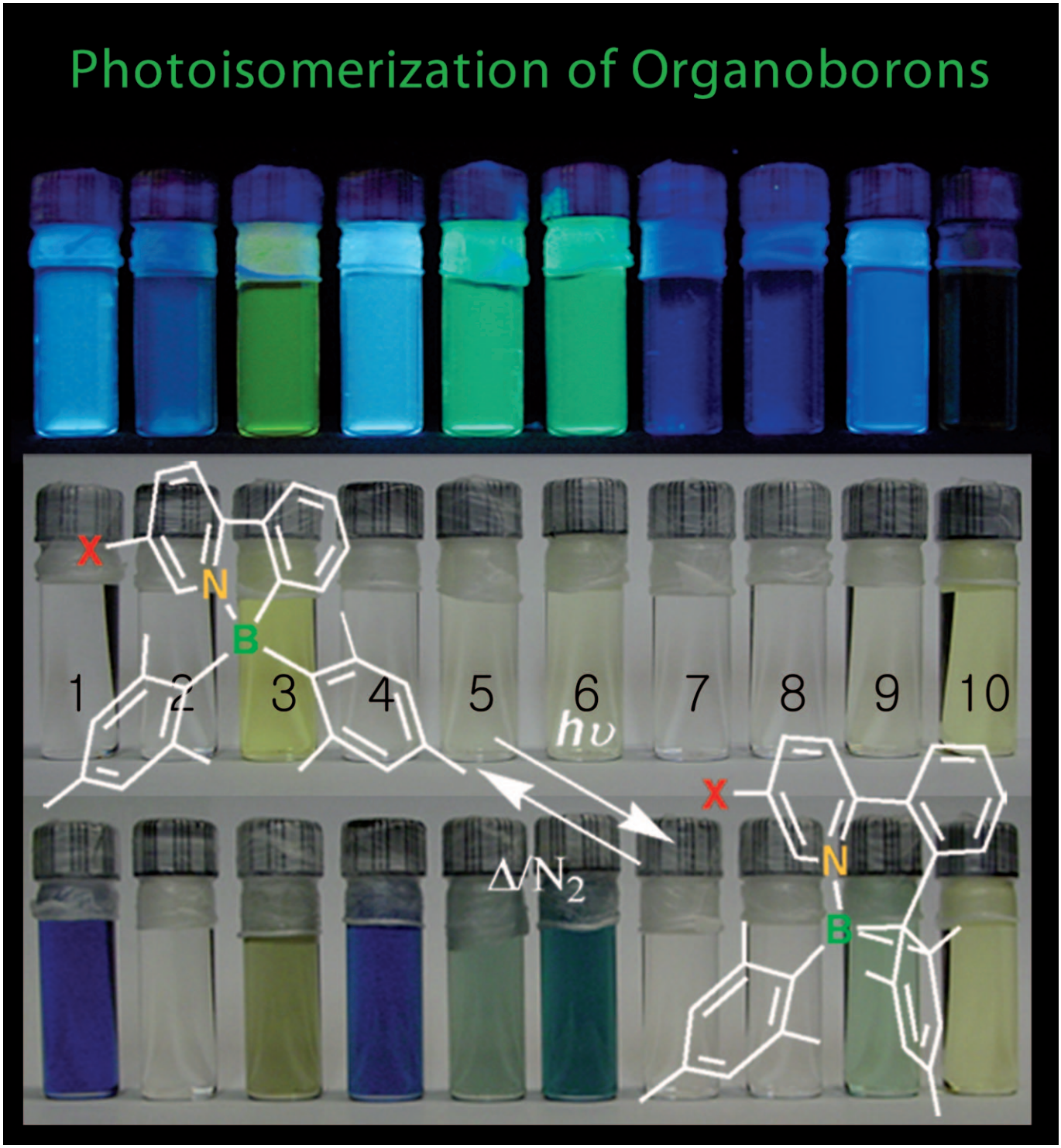

Abstract: A four-coordinate organoboron compound B(ppy)Mes_2 (**1**, ppy = 2-phenylpyridyl, Mes = mesityl) was previously found to undergo reversible photochromic switching through the formation/breaking of a C–C bond, accompanied by a dramatic color change from colorless to dark blue. To understand this unusual phenomenon, a series of new four-coordinate boron compounds based on the ppy-chelate ligand and its derivatives have been synthesized. In addition, new N,C-chelate ligands based on benzo[*b*]thiophenylpyridine and indolylpyridine have also been synthesized and their boron compounds were investigated. The crystal structures of most of the new compounds were determined by X-ray diffraction analysis. UV/Vis, NMR, and electrochemical methods were used to monitor the photoisomerization process. DFT calculations were performed for all compounds to understand the photophysical and electronic properties of this class of molecules. The results of our study showed that the bulky mesityl group is necessary for photochromic switching. Electron-donating and electron-withdrawing groups on the ppy chelate have a distinct impact on the photoisomerization rate and the photochemical stability of the molecule. Furthermore, we have found that the non-ppy-based N,C-chelate ligands such as benzo[*b*]thiophenepyridyl can also promote photoisomerization of the boron chromophore in the same manner as the ppy chelate, but the product is thermally unstable.

Keywords: boron · N ligands · photochemistry · reactivity · structure elucidation

Introduction

Four-coordinate organoboron compounds have been extensively investigated in the past decade as emissive materials for use in organic light-emitting diodes (OLEDs), because of their high thermal and chemical stability.[1,2] In contrast to three-coordinate boron compounds, which can function as a Lewis acid or an electron-transport material in optoelectronic devices through the empty p orbital of the boron center,[3] four-coordinate organoboron compounds can also function as electron-transport materials by means of the boron-stabilized π* orbital of the conjugated chelate ligands.[1,2] We have recently discovered that certain four-coordinate boron compounds such as B(ppy)Mes_2 (**1**, ppy = 2-phenylpyridyl, Mes = mesityl) are not only highly emissive, but also readily undergo an unusual and reversible photochromic switching upon exposure to light (Scheme 1).[4a] We have further discovered that incorporating a second photosensitive chromophore, such as an olefin bond in the N,C-chelate ligand, can inhibit the photoisomerization process by dissipating energy through the alternative *trans–cis* isomerization pathway,[4b] hence enhancing the stability of the four-coordinate boron chromophore. In view of the importance and potential applications of organic photochromic systems[5] and the rarity of photochromic systems based on four-coordinate organoboron compounds, we have conducted a comprehensive study on the ppy-based organoboron compounds. To fully understand the factors influencing the photochromic properties of N,C-chelate four-coordinate boron compounds, we have synthesized a series of analogues with the general formula of B(N,C-L)Ar_2 (**1**–**10**) and various N,C-L ligands and Ar groups. We have found that both steric and electronic factors have a significant impact on the photochromic behavior and photochemical stability of this class of molecules. The details are presented herein.

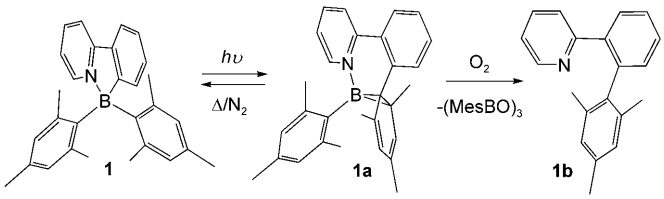

Scheme 1.

Results and Discussion

Syntheses: The organoboron compounds used in this study with the general formula of B(N,C-L)Ar_2 can be classified into two groups depending on the nature of L: group A with a ppy or its derivative as the chelate ligand (compounds **1**–**8**) and group B with other N,C-chelate ligands (**9** and **10**). Compounds in group A can be further divided into two groups based on whether or not the Ar group is a mesityl (**1**–**6**) or a non-mesityl group (**7** and **8**). The syntheses of compounds **1**, **3**, and **5** have been described previously.[4] Compound **2** was prepared according to Scheme 2. Suzuki–Miyaura coupling[6] of 2-bromopyridine with 2,3,4,5-tetrafluorophenyl boronic acid produced the ligand **2′**, which, upon lithiation and the subsequent addition of $BMes_2F$ produced **2** in 39% yield.

The syntheses of compounds **4** and **6** follow a similar procedure, namely the synthesis of the 2-(2-bromophenyl)pyridine derivative and its subsequent reaction with *n*BuLi fol-

[a] H. Amarne, Dr. C. Baik, S. K. Murphy, Prof. Dr. S. Wang
Department of Chemistry
Queen's University, Kingston
Ontario, K7L 3N6 (Canada)
Fax: (+1) 613-5336669
E-mail: wangs@chem.queensu.ca

Supporting information for this article is available on the WWW under http://dx.doi.org/10.1002/chem.200903582.

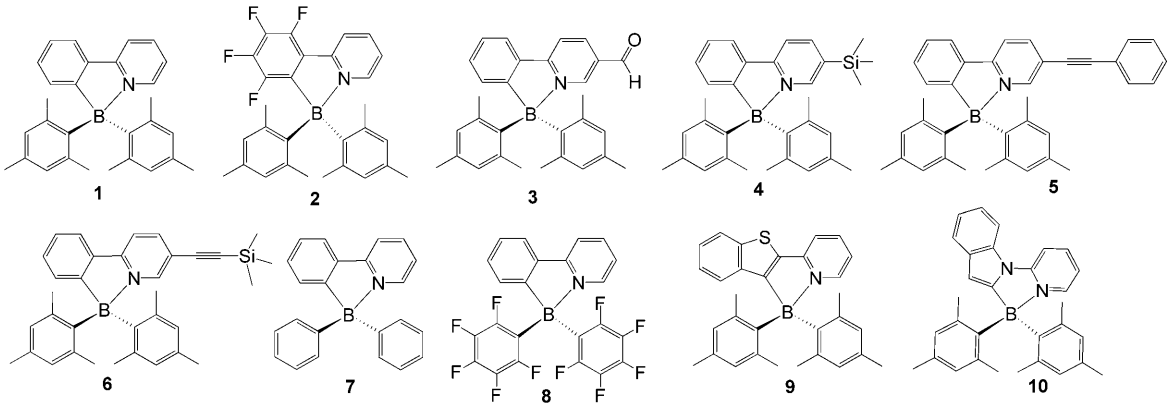

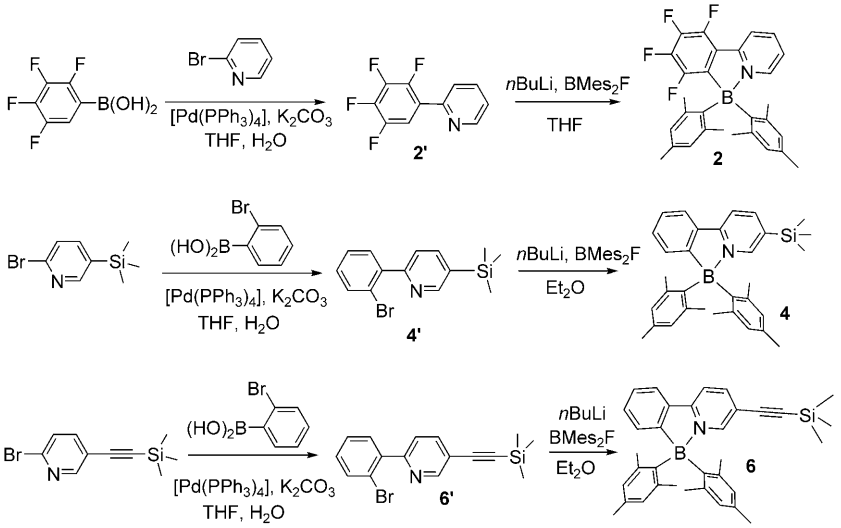

Scheme 2.

lowed by addition of $BMes_2F$, as shown in Scheme 2 (yield 81-83%). The ligand **4′** was obtained by Suzuki–Miyaura coupling of 2-bromo-5-(trimethylsilyl)pyridine with 2-bromophenyl boronic acid. In the same manner, the ligand **6′** was obtained by Suzuki–Miyaura coupling of 2-bromo-5-[2-(trimethylsilyl)ethynyl]pyridine with 2-bromophenyl boronic acid. Compounds **7** and **8** were prepared by lithiation of 2-(2-bromophenyl)pyridine[4a] and the subsequent addition of BPh_2Cl and $(C_6F_5)_2BF$, respectively, as shown in Scheme 3.

Compounds **9** and **10** were prepared according to Scheme 4. The 2-benzo[*b*]thienylpyridine ligand was prepared using a Suzuki–Miyaura coupling reaction of 2-bromopyridine and benzo[*b*]thiophen-2-yl boronic acid. Its subsequent reaction with *n*BuLi and $BMes_2F$ produced **9** in 62% yield. The 2-indolylpyridine ligand, which was prepared by using an Ullmann coupling reaction similar to that for the synthesis of 7-azaindolylpyridine,[7] was treated with LDA followed by addition of $BMes_2F$ to produce **10** in 72% yield. All compounds were fully characterized by NMR spectroscopy, HRMS, and/or elemental analyses.

Crystal structures: The crystal structural data of compounds **1** and **5** were reported previously.[4a,b] The crystal structures of **2**, **4**, and **6**–**9**, determined by single-crystal X-ray diffraction analysis in this work, are shown in Figure 1–3, respectively. The important bond angles and bond lengths of **1**, **2**, **4**–**9** are shown in Table 1 for comparison.

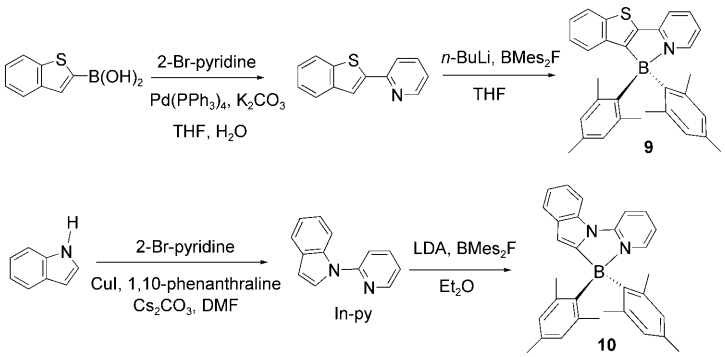

Scheme 4.

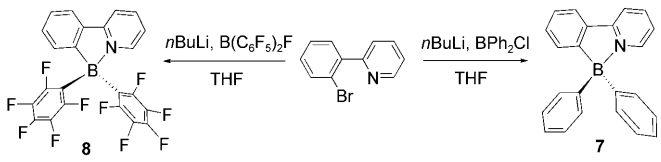

Scheme 3.

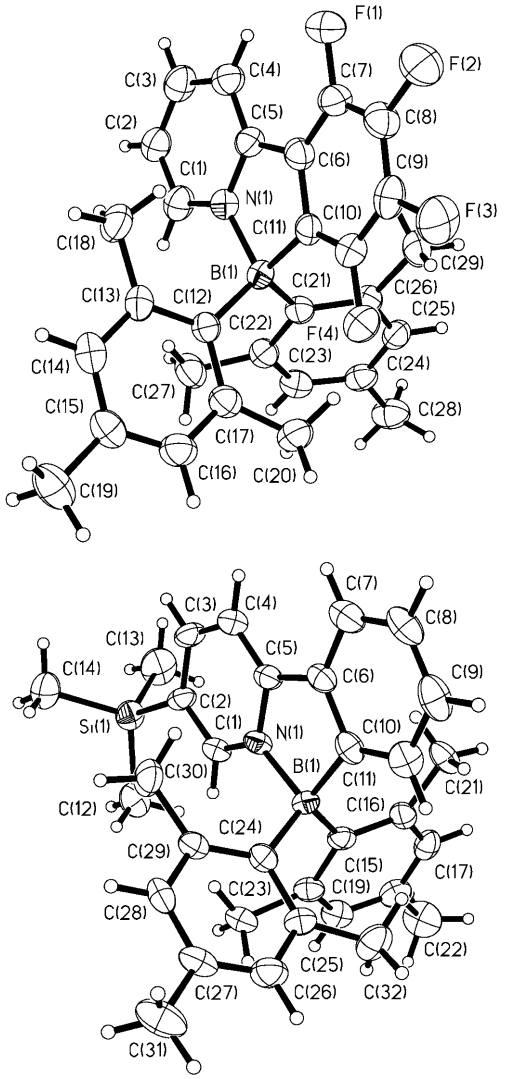

Figure 1. The crystal structures of compound **2** (top) and **4** (bottom) with 50% ellipsoids and labelling schemes.

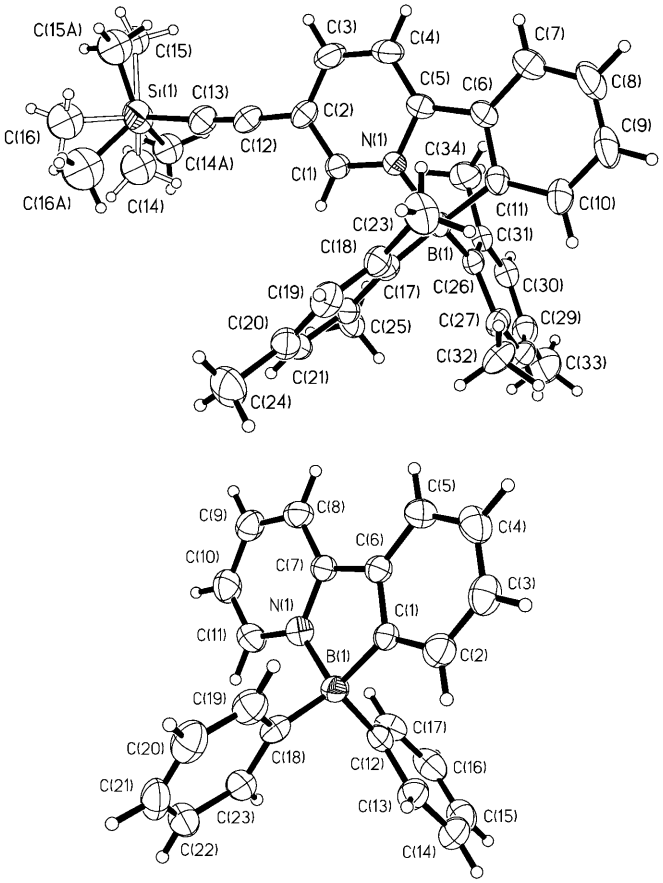

Figure 2. The crystal structures of compound **6** (top, showing the two sets of the disordered $SiMe_3$ group) and **7** (bottom) with 50% ellipsoids and labelling schemes.

Group A: The compounds in group A (**1**–**8**) all contain the ppy or functionalized ppy as the chelate. There are, however, significant variations in B–N and B–C bond lengths among this group of compounds. Comparison of structural data of compound **1** with that of **7** clearly shows that the bulky mesityl groups in **1** destabilize the compound, as evidenced by the much longer B–N (1.653(2) Å) and B–C_{Ar} bonds (1.649(2) Å average)[4a] of **1** versus those of **7** (1.618(3) and 1.613(3) Å, respectively, average) while the C-B-N chelating angle is essentially the same in both compounds. The C_6F_5 group in **8** also destabilizes the molecule relative to the phenyl group in **7** by weakening the B–C_{Ar} bond (1.637(2) Å average). This effect can be attributed to the electron-withdrawing nature of the C_6F_5 group. The electron-donating group $SiMe_3$ in **4**, the phenylacetylene group in **5**,[4b] and the $SiMe_3$-acetylene group in **6** of the ppy chelate do not have significant impacts on the B–C_{Mes} and the B–$C_{chelate}$ bond lengths compared to **1**. In contrast, the electron-withdrawing fluorinated phenyl ring of the ppy chelate in **2** shortens the B–C_{Mes} bond lengths considerably (1.632(5) Å average), while having no significant impact on the B–$C_{chelate}$ bond.

Table 1. Comparison of bond lengths and angles of compounds **1**, **2**, **4**–**9**.

	B–N [Å]	B–$C_{chelate}$ [Å]	B–C_{Ar} [Å]	N-B-$C_{chelate}$ [°]	C_{Ar}-B-C_{Ar} [°]
1	1.6531(19)	1.625(2)	1.644(2) 1.654(2)	95.13(10)	114.91(11)
2	1.661(4)	1.628(5)	1.629(5) 1.636(5)	94.5(2)	116.1(3)
4	1.638(5)	1.639(6)	1.648(5) 1.649(6)	95.2(3)	115.9(3)
	1.643(6)	1.641(6)	1.633(6) 1.661(5)	95.1(3)	116.3(3)
5	1.642(3)	1.631(4)	1.650(4) 1.650(4)	95.44(18)	115.3(2)
6	1.667(4)	1.621(4)	1.632(5) 1.643(5)	95.2(4)	115.6(2)
7	1.618(3)	1.628(3)	1.611(3) 1.616(3)	95.58(13)	113.48(15)
8	1.612(2)	1.610(2)	1.635(2) 1.639(2)	97.63(11)	114.34(12)
9	1.659(6)	1.617(6)	1.632(7) 1.633(7)	94.8(4)	116.2(4)

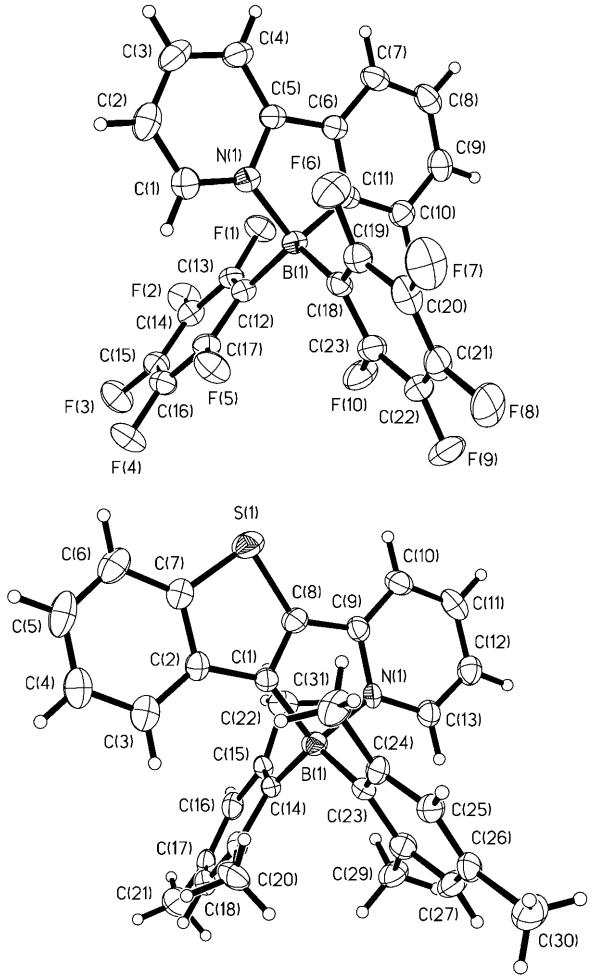

Figure 3. The crystal structures of compound **8** (top) and **9** (bottom) with 50% ellipsoids and labelling schemes.

Group B: The structure of compound **9** provides an important comparison of non-ppy-based N,C-chelate ligands with those of ppy and derivatives. Comparison of the structural data of **9** and **1** shows that the B–C_{Mes} bonds in **9** (1.632(7) Å average) are shorter, while the B–N and B–$C_{chelate}$ bond lengths are similar for both compounds. Nonetheless, the overall structural features of **9** resemble those of **1**. The crystal structure of **10** was not determined due to the lack of adequate crystals.

The crystal structural data indicates that despite the bulky mesityl groups in compounds **1**–**6** and **9** and **10**, the boron center retains a four-coordinate environment similar to that of the phenyl and pentafluorophenyl compounds **7** and **8** in the solid state. In solution, these compounds also retain the four-coordinate geometry, as confirmed by their ^{11}B chemical shift.[8] In addition, unlike three-coordinate triarylboron compounds that readily react with fluoride ions,[3] compounds **1**–**10** do not show any reactivity with fluoride ions, as established by an NMR study (see Supporting Information), further supporting their four-coordinate geometry in solution.

Photophysical and electrochemical properties: UV/Vis absorption spectra and fluorescence spectra for compounds **1**–**10** are shown in Figure 4. The λ_{max} of the lowest energy absorption band, the absorption edge (optical energy gap), and the λ_{max} of the emission spectra along with fluorescence quantum efficiencies are provided in Table 2. All compounds have intense absorption bands at 290–400 nm. For the mesityl compounds **1**–**6**, **9**, and **10**, there is a low-energy shoulder in the 350–470 nm region that can be attributed to

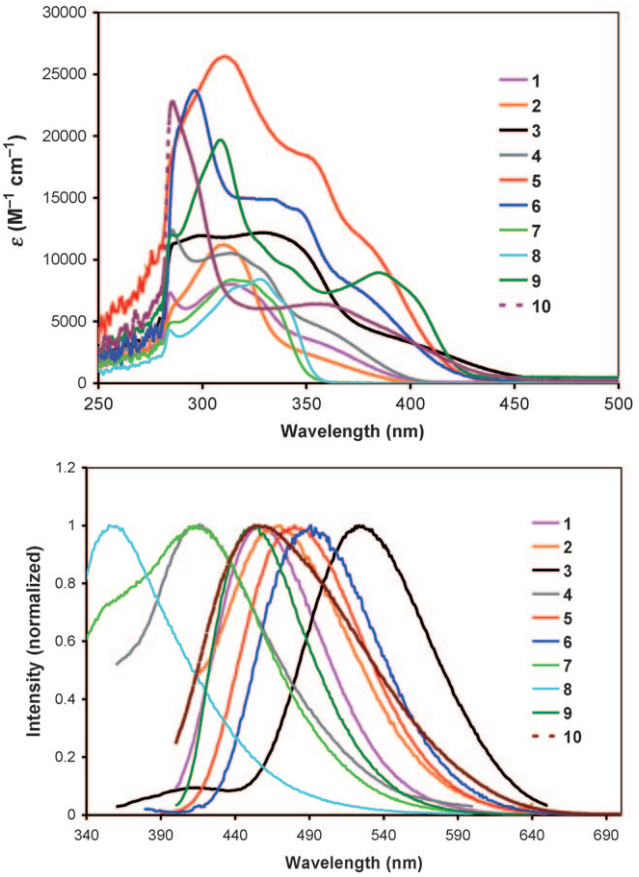

Figure 4. Top: UV/Vis spectra recorded in toluene ($\approx 10^{-5}$ M) . Bottom: fluorescence spectra recorded in toluene ($\approx 10^{-5}$ M).

Table 2. Photophysical and electrochemical properties of **1**-**10** in toluene ($\approx 10^{-5}$ M).

	Absorption λ_{max} [nm] (ε [$M^{-1}cm^{-1}$])	Optical energy gap [eV]	λ_{em} [nm]	Φ in toluene[a]	$E^{red}_{1/2}$ [V][b]
1	357 (3207)	3.10	458	0.10	−2.30
2	349 (2397)	3.13	470	0.05	−2.09
3	390 (3780)	2.70	527	0.15	−1.68
4	355 (4672)	3.08	418	0.12	−2.32
5	377 (11726)	2.90	490	0.37	−2.03
6	371 (8161)	2.93	490	0.28	−2.04
7	334 (6503)	3.51	413	0.31	−2.28
8	341 (6164)	3.48	360	0.22	−2.09
9	386 (8923)	2.89	455	0.30	−2.19
10	362 (6264)	2.81	461	0.024	−2.23

[a] Determined using 9,10-diphenylanthracene as the standard. [b] From CV diagrams recorded in DMF, relative to the potential of $FeCp_2^{+/0}$.

a charge-transfer transition from the mesityl to the ppy chelate based on the results of our previous study of compounds **1** and **5**.[4] The fact that this low-energy shoulder is absent in the absorption spectra of the non-mesityl compounds **7** and **8** is consistent with this assignment. The phenyl and pentafluorophenyl compounds **7** and **8**, respectively, have the largest optical energy gap. All compounds except **10** are either modest or bright fluorescent emitters with λ_{max} ranging from 360 to 527 nm (Figure 4). The emission energy of compounds **1**–**4** follows the order of **4**>**1**>**2**>**3**, which is also in agreement with a charge-transfer transition from the mesityl π to the ppy-chelate π* level, since an electron-donating $SiMe_3$ group in **4** raises the π* level of the ppy, while an electron-withdrawing group, such as the carbonyl in **3**, stabilizes it. Extended π-conjugation of the ppy chelate with an acetylene group also significantly decreases the energy of the charge-transfer transition due to the stabilization of the π* level, as evidenced by the much longer emission wavelength of compounds **5** and **6**, relative to that of **1**. The benzo[*b*]thienylpyridine compound **9** is a bright emitter at a wavelength similar to that of **1**, while the indolylpyridine compound **10** emits in the same region, but much more weakly.

In the cyclic voltammetry diagrams, all compounds display a reduction peak that can be attributed to the reduction of the π* orbital of the N,C-chelate ligand (Figure 5). Compound **1** has a reduction peak at −2.30 V (vs. $FeCp_2^{+/0}$), which is much more negative than those of the triarylboron isomers[9] of **1**, 2-(4-$BMes_2$-C_6H_4)pyridine (−2.16 V) and 5-$BMes_2$-2-C_6H_5-pyridine (−2.12 V), indicating that triarylborons are better electron acceptors. Electron-withdrawing groups such as fluoro and carbonyl groups (**2** and **3**) greatly shift the reduction potential to more positive values, while the electron-donating group $SiMe_3$ (**4**) shifts the potential to a more negative value. The π conjugation of the acetylene group in the ppy ligand (**5**, **6**) also shifts the reduction potential to more positive values, relative to that of **1**. These observations are all consistent with the LUMO level being the π* orbital of the ppy chelate. The diphenyl compound **7** has a similar reduction potential as that of **1**, despite the weaker N,C-chelating bonds in **1** that should destabilize the π* level somewhat. The pentafluoro compound **8** has a much more positive reduction potential than that of **1**. This can be attributed to the greater σ donation of the ppy ligand to the boron center, as evidenced by the much shorter B−N and B−$C_{chelate}$ bond lengths in **8** (Table 1), which causes stabilization of the π* level. This supports the fact that the nature of the aryl group has an impact on the π* level of the chelate moiety due to their influence on the electron density of the B center. The non-ppy-chelate compound **9** has a more positive reduction potential than **1**, which is attributable to the greater π conjugation. Compound **10**, however, has a potential similar to that of **1**, despite the much bigger indolylpyridine chelate ligand. It is worth noting that compounds **2** and **10** are unstable toward electrochemical reduction even in the absence of light, as evidenced by the appearance of new species in the CV diagrams after reduction (see Supporting Information), while compounds **1**, **3**, **4**, and **6** have the best stability toward reduction. The reduction potentials for all compounds are provided in Table 2.

DFT calculations for compounds 1–10: Our previous TD-DFT computations[4] on compounds **1** and **5** established that the HOMO–LUMO (mesityl to ppy) transition is responsible for the lowest energy transition observed in the absorption and emission spectra for these two compounds. It is therefore reasonable to assume that the same is true for the new dimesitylboron compounds. Hence, only non-time-dependent DFT calculations were performed for the new compounds to validate the general trend of the experimentally observed photophysical properties of this class of molecules. The calculated HOMO–LUMO energies and gaps along with the experimental values determined from CV and absorption data are provided in Figure 6. The data show that

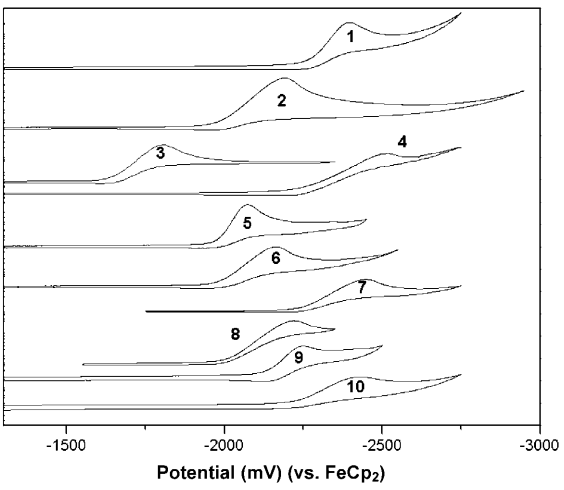

Figure 5. The CV diagrams showing the reduction peak of compounds **1**–**10**, recorded in DMF with scan rates 200 or 300 mV s^{-1}.

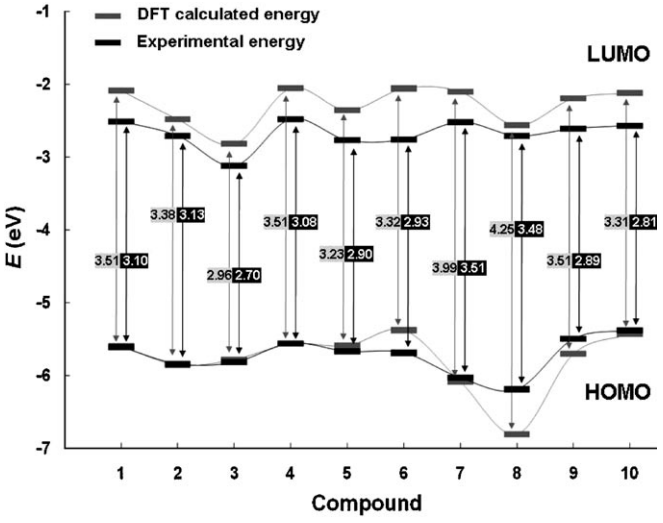

Figure 6. The calculated and experimental HOMO–LUMO energy levels of compounds **1**–**10**.

the general trend of the calculated HOMO and LUMO energies agree with the experimentally observed trend. The HOMO and LUMO diagrams of all new compounds are provided in the Supporting Information. For all molecules, the HOMO level is mainly concentrated on one of the aryl groups, while the LUMO level exclusively nearly involves the π^* orbital of the N,C-chelate group. Thus, the lowest energy electronic transition in all molecules can be considered a charge-transfer transition from the aryl group to the N,C-chelate unit. For compounds **7** and **8**, this transition most likely overlaps with the $\pi \rightarrow \pi^*$ transition localized on the ppy chelate, leading to the absence of a low-energy shoulder in the absorption spectra. The large HOMO–LUMO gaps in **7** and **8** are clearly due to the deep HOMO levels caused by the phenyl and the pentafluorophenyl groups, respectively, relative to that of mesityl. Some of the large discrepancies between calculated and experimental values can be attributed to the limitation of the ground state DFT calculations.

Photochromic properties: Compounds **1**–**10** display distinct responses toward irradiation by light. For example, compounds **3**, **4**, **6**, and **9** undergo photochromic switching from either colorless or light yellow to dark blue or dark green upon irradiation by UV light (350 or 365 nm) under nitrogen (Figure 7). This phenomenon is reminiscent of the photochromism of compounds **1** and **5**, which have been shown previously to change color from colorless or light yellow to dark blue upon irradiation by UV light through the formation of the species **1a** and its analogue **5a**, respectively (Scheme 1).[4] Indeed, UV/Vis (Figure 8) and ^{1}H NMR spectral data (see Supporting Information). confirmed that compounds **3**, **4**, **6**, and **9** form the same type of species as **1a** and **5a** upon irradiation. In contrast, the diphenyl compound **7** and the pentafluorophenyl compound **8** are stable toward UV irradiation at either 350 or 310 nm and no photochromic

Figure 7. Photographs of compounds **1**–**10** in toluene showing their colors (middle), fluorescent colors (top), the color change after being irradiated by a UV lamp (365 nm) for ≈5 min for **1**, **3**, **4**, and **6** and ≈20 min for all other compounds (bottom).

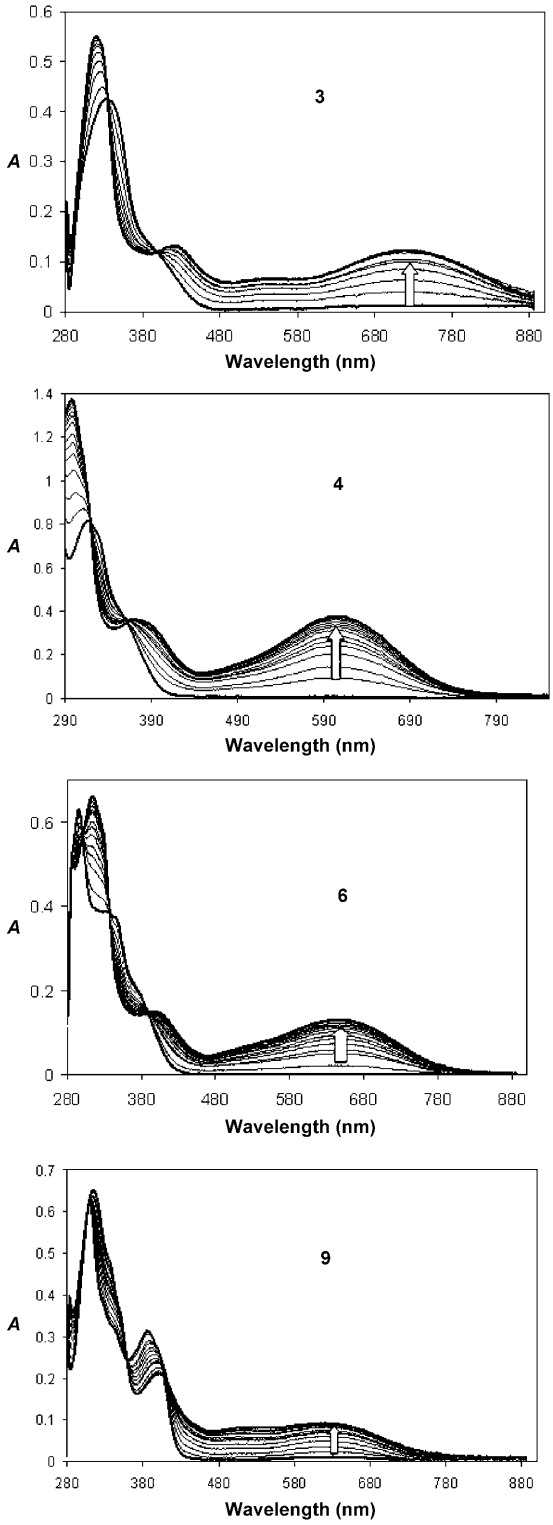

Figure 8. The UV/Vis spectral change of compound **3**, **4**, **6**, and **9** in toluene after being exposed to UV light (365 nm). The spectra were recorded at 5 seconds intervals for **3**, **4**, and **9** and 3 seconds for **6** of UV exposure.

switching was observed, while compounds **2** and **10** undergo decomposition upon irradiation at 350 nm.

Steric factor: The key difference between compound **7** and **1** is that the former has two phenyl groups, while the latter has two mesityl groups attached to the boron center. Crystal structural data indicated that the B–mesityl bonds in **1** are much longer than those of the B–C_6H_5 bonds in **7** owing to the fact that mesityl groups are much bulkier than phenyl groups. The weaker B–mesityl bonds and the electron-donating methyl groups are clearly responsible for the low-energy charge-transfer transition from the mesityl→ppy in **1** with respect to the phenyl→ppy transition in **7**. Nonetheless, the lack of any photochromic switching of **7**, even under irradiation at 310 nm that is near the λ_{max} of its low-energy absorption band, suggests that the steric congestion in **1** is likely the key factor responsible for the photochromic properties of **1**. The non-photoresponsive behavior of **7** and **8** is also in sharp contrast to that of BPh_4^- and BPh_3(biphenyl)$^-$, which are known to produce C–C coupled products with the formation of a BC_2 ring upon irradiation at 254 nm.[10] The greater photochemical stability of **7** and **8** versus that of BPh_4^- or BPh_3(biphenyl)$^-$ can only be attributed to the ppy-chelate ligand.

Chelate ligands: Compounds **9** and **10** are the only members that do not have ppy or its derivative as the chelate ligand. The N,C-chelate units in both molecules involve a pyridyl and a five-membered thiophene or pyrrole ring. Compound **9** undergoes a photochromic switching process similar to that of **1**. In the presence of oxygen, the C–C coupled product **9b**—an analogue of **1b** shown in Scheme 1—was isolated and fully characterized by NMR and MS analyses. This demonstrates that the photochromic switching and C–C coupling phenomenon is not limited to the ppy-chelate chromophore. Using **1** as the internal standard, a competitive photolysis experiment at 365 nm monitored by NMR spectroscopy established that the rate of photoisomerization of **9** to **9a** is much slower than that of **1** and the ratio of the relative rate constants of $k(\mathbf{1})/k(\mathbf{9})$ was determined to be $\approx$15 (see Supporting Information), despite the much greater absorbance of **9** at 365 nm. The slower conversion of **9** to **9a** relative to **1** to **1a** can be attributed to the greater π conjugation of the benzo[*b*]thiophenepyridyl chelate, which stabilizes the excited state and enhances the radiative decay pathway. This explanation is supported by the significantly higher quantum efficiency of **9** compared to that of **1**, as shown in Table 2.

In contrast to compound **9**, the indolylpyridyl chelate compound **10** undergoes decomposition upon irradiation instead of photoisomerization. The C–C coupled product **10b** was not observed when the photolysis was conducted under air. Although we were not able to obtain a single-crystal structure for **10**, the structure of a closely related compound B[5-(7-azaindolyl)-2-Br-py]Mes_2 was determined (see Supporting Information) which has a Mes-B-Mes angle of 120.2(3)°—the largest among this group of compounds. In addition, the B–N (1.660(5) Å) and B–$C_{chelate}$ (1.650(6) Å) bond lengths in B[5-(7-azaindolyl)-2-Br-py]Mes_2 are also among the longest. Due to the similarity of the azaindolylpyridyl and indolylpyridyl chelate ligands, it is reasonable to assume that compound **10** likely possesses the same structural characteristics. Hence, the poor photochemical stability of **10** is likely due to the poor stability of the indolylpyridyl chelate.

Electronic factor: To investigate the impact of electron-donating and electron-withdrawing groups on photoisomerization of the ppy-chelate compounds, we compared the photoisomerization rate of **3** and **4** relative to that of **1**. For compound **3**, the photoisomerization rate is somewhat smaller than that of **1** ($k(\mathbf{1})/k(\mathbf{3})\approx1.2$), as determined by the competitive photolysis NMR experiments in C_6D_6 However, complete conversion of **3** to **3a** could not be achieved due to the decomposition of **3** after extended exposure to UV irradiation. For **4**, the isomerization rate is faster than **1** with $k(\mathbf{1})/k(\mathbf{4})\approx0.80$ and the full conversion to **4a** can be achieved readily. As shown in Figure 6, the electron-donating group $SiMe_3$ destabilizes the π* level, hence destabilizing the excited state, which appears to accelerate the photoisomerization process. Compounds **5** and **6** have an acetylene group attached to the ppy and both compounds can be fully converted to **5a** and **6a**, respectively. The rate of conversion of compound **6** was found to be similar to that of **4** ($k(\mathbf{1})/k(\mathbf{6})\approx0.80$), while the rate for **5** is much slower than that of **1** ($k(\mathbf{1})/k(\mathbf{5})\approx20$). The extended π conjugation of the chelate ligand with the phenyl group is believed to be responsible for the slow photochromic response of **5**, as is the case for compound **9**. The similar photoisomerization rates of **4** and **6** suggest that the electron donating effect by the –CC–$SiMe_3$ group in **6** may be dominant. The ratio of the photoisomerization rate constants of **1**/**1a** and **5**/**5a** were previously determined to be about 20[4b] by UV/Vis spectroscopy, which agrees well with the value determined here by the NMR experiments. Using the absorbance data and the relative rate constants,[12] the relative photoisomerization quantum efficiency of **1** versus that of **3**–**6** and **9** was estimated to be approximately 2.5, 1.2, 74, 2.2, and 36, respectively, under NMR photolysis conditions. Thus, compound **1**, the simplest in this group of compounds, is the most efficient in the photoisomerization process.

The C–C coupled products **3b**–**6b**—analogues of **1b**—were obtained by either exposing **3a**–**6a** to air, or by irradiating solutions of **3** or **4** in benzene or toluene in the presence of O_2, and have been identified and characterized by MS analyses. This further supports that these compounds undergo photoisomerization in the same manner as **1** does. In addition, the photoisomerizations of **4**–**6** are also fully reversible and thermally slow at ambient temperature and fast upon heating to 70 °C, as is the case for compound **1** (see Supporting Information). Compound **9a** does not reverse back to **9** at ambient temperature. Heating the solution of **9a** in benzene or toluene at 70 °C led to unidentified decomposition products (see Supporting Information), an indica-

tion that compound **9a** may be thermally unstable. Attempts to reverse the photoisomerization process by using visible light have not been successful. The fluoro-substituted compound **2** was found to be unstable toward photolysis and an insoluble orange solid was observed after the solution of **2** in benzene or toluene was irradiated by UV light under the same conditions as for **1**, and **3**–**6**. The fluoro substituents on the phenyl ring are clearly responsible for the photochemical instability of the molecule, although the exact cause is not known. Our attempts to synthesize mono- and difluoro-substituted analogues to better understand this phenomenon were unsuccessful due to difficulties in controlling the lithiation site on the fluoro-substituted phenyl ring.

Photophysical and electrochemical properties of the dark species: The dark colored species of **1a**, **3a**–**6a**, and **9a** are characterized by one intense and broad absorption band in the visible region, as shown in Figure 8. Compound **3a** has the longest absorption wavelength (728 nm), while compounds **1a** and **4a** have the shortest wavelength (605 nm). Previous TD-DFT calculation results[4a] for **1a** showed that its HOMO is dominated by the "bent bonds"[11] of the BC_2 ring between the B and the C atoms and the π orbitals of the cyclohexadienyl ring, while its LUMO is mostly the π* of the ppy chelate. In addition, TD-DFT results confirmed that the dark color of **1a** arises predominately from the HOMO to LUMO transition. The observed trend of the absorption band of **1a**, **3a**–**6a**, and **9a** is consistent with this transition assignment.

The dark colored species of **1a**, **3a**, **4a**, and **6a** can also be detected readily by electrochemical analysis. As shown in Figure 9, a distinct oxidation peak appears at about −0.50 V (vs. $FeCp_2^{+/0}$) in the CV diagram during irradiation that grows in intensity with exposure time. Because this peak is absent when the UV lamp is off, it can be assigned to the species of **1a**, **3a**, **4a**, and **6a**, which are generated by photoisomerization. For **1**, **4**, and **6**, we were able to obtain the CV diagrams representing the pure species **1a**, **4a**, and **6a**, because of the fast photoisomerization. The reduction peaks of **1a**, **4a**, and **6a** appear at a similar potential as those of **1**, **4**, and **6**, indicating that the LUMO energy level does not change significantly upon isomerization, which is consistent with the TD-DFT results obtained for **1** and **1a**.[4a] The low oxidation potentials of **1a**, **3a**, **4a**, and **6a** indicate that the dark species have a high HOMO level (−4.26, −4.30, −4.28, and −4.31 eV, respectively), thus explaining their high susceptibility toward oxidation by oxygen. The electrochemical energy gaps of **1a**, **3a**, **4a**, and **6a**, obtained from the reduction and the oxidation potentials, follow the same trend as that of the optical energy gaps obtained from the absorption edge as shown in Table 3. For compounds **5** and **9**, it was not possible to detect the dark species conclusively in the CV diagram due to the very slow conversion of **5** and **9** to **5a** and **9a**.

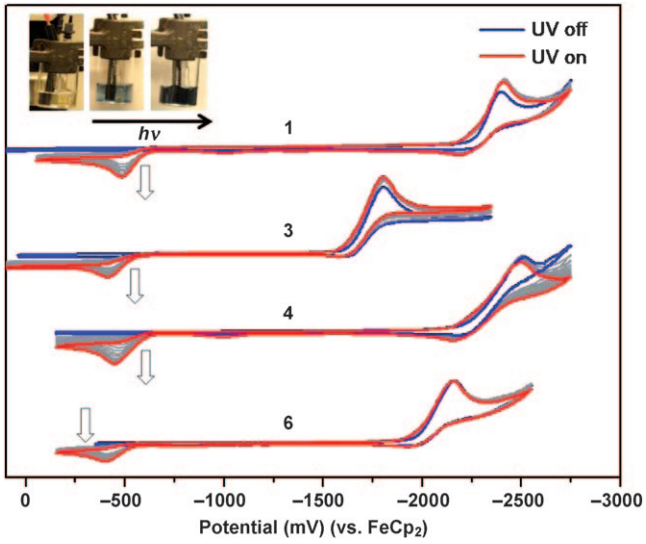

Figure 9. CV diagrams of **1**, **3**, **4**, and **6** before and after UV irradiation (365 nm) in DMF with NBu_4PF_6 as the electrolyte and 200 $mV s^{-1}$ scan rate. Inset: Photographs showing the color change of the solution of compound **6** in the electrochemical cell with and without exposure to UV light.

Table 3. Photophysical and electrochemical data of **1a**, **3a**–**6a**, and **9a**.

	Absorption[a] λ_{max} [nm]	Optical energy gap [nm eV^{-1}]	$E^{ox}_{1/2}$ [V][b]	$E^{red}_{1/2}$ [V][b]	Electrochemical energy gap [eV]
1a	605	770/1.61	−0.54	−2.30	1.76
3a	728	≈930/≈1.33	−0.50	−1.68	1.18
4a	605	770/1.61	−0.52	−2.32	1.80
5a	640	820/1.51	−0.51	−2.03	1.52
6a	650	825/1.50			
9a	628	800/1.55			

[a] Recorded in toluene (≈1.0^{-5} M). [b] Recorded in DMF, relative to the potential of $FeCp_2^{+/0}$.

Conclusion

Based on the results of this study, we suggest the following.

1) The photoisomerization of the N,C-chelate four-coordinate boron compounds is most likely initiated by a photoinduced charge transfer from the HOMO localized on the aryl group to the LUMO localized on the chelate unit.
2) The bulky mesityl groups are required to observe the photoisomerization phenomenon of the ppy-based four-coordinate boron compounds, which can be attributed to the destabilization of the molecule and the HOMO level by the bulky mesityl. Other bulky aryl groups most likely have the same impact on the photoisomerization of N,C-chelate boron chromophores, which should be a topic of future work.
3) Electron-donating groups such as $SiMe_3$ on the ppy chelate appear to accelerate the photoisomerization rate by destabilizing the excited state.
4) Extended π conjugation on the ppy chelate appears to retard the photoisomerization process by stabilizing the excited state.

5) Electron-withdrawing groups, such as fluoro or carbonyl groups on the ppy chelate, appear to either slow down the photoisomerization process and/or cause irreversible photodecomposition of the molecule, and thus these substitution patterns may not be desirable for achieving stable and reversible photoswitching systems.
6) The photoisomerization is not limited to the ppy-chelate system, as demonstrated by compound **9**. However, the boron compounds based on the non-ppy-chelate ligands benzo[*b*]thiophenepyridyl or indolylpyridyl have either a poor thermal reversibility for the photoisomerization process or decompose upon photolysis, thus making them unsuitable for use in photochromic systems.

Although it is not clear yet whether or not other unexplored N,C-chelate ligands will perform better, the ppy-based compounds are most promising as reversible photothermal switching materials. Compound **1**, the simplest member of the ppy group, is the most efficient in the photoisomerization process, among all the compounds that have been examined by our group.

Experimental Section

General: Starting materials were purchased from Aldrich Chemical Co. and were used with out further purification. Solvents were dried using an activated alumina column system, purchased from Innovative Technology Inc., while C_6D_6 was dried over CaH_2 in a glove box. All reactions were carried out under an atmosphere of dry nitrogen using standard Schlenk techniques. Purifications using column chromatography were performed using ultra pure silica gel (70–230 Mesh) 60 Å, purchased from Silicycle. NMR spectra (^{1}H,^{13}C, ^{11}B, and ^{19}F) were recorded at room temperature on a Bruker Avance 400 or 500 MHz. Proton and ^{13}C chemical shifts were reported with respect to solvent peaks as internal standard, while $BF_3.Et_2O$ and $CFCl_3$ were used as references for ^{11}B and ^{19}F NMR signals, respectively. Excitation and emission spectra were recorded on a Photon Technologies International QuantaMaster Model C-60 spectrometer. UV/VIS spectra were recorded on an Ocean Optics Model CHEM-USB4-UV/VIS. Elemental analyses were performed by Canadian Microanalytical Services Ltd. Delta, BC. Cyclic voltammetry was performed using a BAS CV-50W analyzer with a scan rate of 200 mV s^{-1} and sample concentrations of 5 mg/3.0 mL DMF, using 0.10 M NBu_4PF_6 (TBAP) as supporting electrolyte and Ag/AgCl reference electrode. The ferrocenium/ferrocene couple was used as the internal standard (E^o = 0.56 V). 2-(2-Bromophenyl)pyridine,[4a] 2-bromo-5-(trimethylsilyl)pyridine,[13] 6-bromonicotinaldehyde,[14] $B(C_6F_5)_2F$,[15] BPh_2Cl,[16] compounds[4] **1**, **3**, and **5** were synthesized by previously reported procedures. Synthetic procedures for all N,C-chelate ligands are provided in the supporting information.

General procedure for preparation of the 2-[2-(dimesitylboryl)phenyl]-pyridines: *n*BuLi (1.6 M in hexane, ca. 1.1 equiv for all compounds except **10** for which LDA was used) was added slowly to a solution of phenylpyridine ligands (1 equiv) in THF (or Et_2O), at −78 °C; the resulting solution was stirred for 1 h at −78°. Then, diaryl boron halide (1.3 equiv) was added quickly under nitrogen and the solution was stirred at the same temperature for 2 h and then stirred overnight at ambient temperature. After the solution was extracted with H_2O/diethyl ether, the crude product was purified by column chromatography using hexane/CH_2Cl_2 to afford the pure product.

Compound 2: 2-(2,3,4,5-Tetrafluorophenyl)pyridine (0.087 g, 0.38 mmol) in THF (30 mL), *n*BuLi (1.6 M in hexane, 0.24 mL, 0.38 mmol), and $BMes_2F$ (0.114 g, 0.38 mmol) were treated as described in the general procedure. Yellow crystals of **2** were obtained (0.07 g, 39 %). ^{1}H NMR (CD_2Cl_2): δ = 8.72 (d, J = 6.0 Hz, 1H), 8.29 (d, J = 8.0 Hz, 1H), 8.12 (t, J = 7.8 Hz, 1H), 7.41 (t, J = 6.6 Hz, 1H), 6.69 (s, 4H), 2.19 (s, 6H), 1.80 ppm (s, 12H); ^{13}C NMR (CD_2Cl_2): δ = 154.2, 148.4–148.3 (m), 146.3, 146.0–146.1 (m), 143.9–143.8 (m), 141.9, 140.6, 137.9–137.8 (m), 134.9, 130.4, 123.4, 122.6 (d, $J_{C.F}$ = 12.6 Hz), 24.6, 20.6 ppm; ^{19}F NMR (CD_2Cl_2): δ = −129.9 (t, J_F = 20.9 Hz, 1F), −144.4 (td, J_F = 20.5, 4.9 Hz, 1F), −152.2 to −152.4 (m, 1F), −161.6 ppm (t, J_F = 19.4 Hz, 1F); ^{11}B NMR (CD_2Cl_2): δ = 8.08 ppm; HRMS: *m*/*z* calcd for $C_{29}H_{26}BF_4N$: 475.2028 $[M]^+$; found: 475.2093; elemental analysis calcd (%) for $C_{29}H_{26}BF_4N$: C 73.28, H 5.51, N 2.95; found: C 73.08, H 5.61, N 2.91.

Compound 4: 2-(2-Bromophenyl)-5-(trimethylsilyl)pyridine (0.64 g, 2.10 mmol) in Et_2O, *n*BuLi (1.60 M in hexane, 1.43 mL, 2.30 mmol), and at $BMes_2F$ (0.71 g, 2.64 mmol) were treated as described in the general procedure. Colorless crystals of **4** were obtained (0.81 g, 81 %). ^{1}H NMR (CD_2Cl_2): δ = 8.68 (s, 1H), 8.09 (d, J = 8.0 Hz, 1H), 8.00 (d, J = 8.0 Hz, 1H), 7.91 (d, J = 6.8 Hz, 1H), 7.74 (d, J = 6.8 Hz, 1H), 7.31–7.27 (m, 2H), 6.65 (s, 4H), 2.17 (s, 6H), 1.79 (s, 12H), 0.28 ppm (s, 9H); ^{13}C NMR ($CDCl_3$): δ = 159.2, 150.0, 145.6, 140.0, 135.4,133.9, 133.7, 131.2, 130.1, 125.5, 122.0, 117.6, 24.9, 20.7, −1.67 ppm; ^{11}B NMR (CD_2Cl_2): δ = 7.21 ppm; HRMS: *m*/*z* calcd for $C_{32}H_{38}BNSi$: 475.2867 $[M]^+$; found: 475.2867; elemental analysis calcd (%) for $C_{32}H_{38}BNSi$: C 80.82, H 8.05, N 2.95; found: C 80.70, H 7.99, N 2.97.

Compound 6: 2-(2-Bromophenyl)-5-[(trimethylsilyl)ethynyl]pyridine (0.25 g, 0.76 mmol), *n*BuLi (1.60 M in hexane, 0.57 mL, 0.91 mmol), and $BMes_2F$ (0.27 g, 1 mmol) were treated as described in the general procedure. Yellow crystals of **6** were obtained (0.31 g, 83 %). ^{1}H NMR ($CDCl_3$): δ = 8.69 (s, 1H), 7.98 (d, J = 8.0 Hz, 1H), 7.90 (d, J = 8.0 Hz, 1H), 7.81 (d, J = 7.2 Hz, 1H), 7.79 (d, J = 7.2 Hz, 1H), 7.32 (d, J = 7.2 Hz, 1H), 7.27 (d, J = 7.2 Hz, 1H), 6.68 (s, 4H), 2.21 (s, 6H), 1.79 (s, 12H), 0.27 ppm (s, 9H); ^{13}C NMR ($CDCl_3$): δ = 166.7, 158.7, 149.4, 145.5, 143.5, 140.6, 134.8, 134.4, 132.2, 131.6, 130.3, 125.9, 122.3, 118.5, 117.6, 100.9, 100.1, 25.4, 21.2, 0.1 ppm; ^{11}B NMR (CD_2Cl_2): δ = 7.93 ppm; HRMS: *m*/*z* calcd for $C_{34}H_{38}BNSi$: 499.2867 $[M]^+$; found: 499.2891; elemental analysis calcd (%) for $C_{34}H_{38}BNSi$: C 81.74, H 7.67, N 2.80; found: C 82.91, H 7.81, N 2.83.

Compound 7: 2-(2-Bromophenyl)pyridine (1.17 g, 5.0 mmol) in THF (50 mL), *n*BuLi (1.6 M in hexane, 3.13 mL, 5.0 mmol), and BPh_2Cl (1.1 g, 5.0 mmol) were treated by the general procedure. Colorless crystals of **7** were obtained (0.52 g, 33 %). ^{1}H NMR (CD_2Cl_2): δ = 8.52 (dt, J = 5.6 Hz, J = 1.2 Hz, 1H), 8.20–8.05 (m, 2H), 7.96 (d, J = 8.0 Hz, 1H), 7.71 (d, J = 7.2 Hz, 1H), 7.55–7.42 (m, 2H), 7.38 (td, J = 7.4 Hz, J = 1.2 Hz, 1H), 7.30–7.10 ppm (m, 10H); ^{13}C NMR (CD_2Cl_2): δ = 158.6, 144.3, 141.2, 136.4, 133.2, 131.3, 130.7, 127.6, 126.3, 125.9, 122.5, 122.1, 118.7 ppm; ^{11}B NMR (CD_2Cl_2): δ = 6.48 ppm; HRMS: *m*/*z* calcd for $C_{23}H_{18}BN$: 319.1532 $[M]^+$; found: 319.1530; elemental analysis calcd (%) for $C_{23}H_{18}BN$: C 86.54, H 5.68, N 4.39; found: C 86.46, H 5.81, N 4.42.

Compound 8: 2-(2-Bromophenyl)pyridine (0.58 g, 2.5 mmol) in THF (50 mL), *n*BuLi (1.6 M in hexane, 1.56 mL, 2.5 mmol), and $B(C_6F_5)_2F$ (2.5 mmol based on 100 % yield) were treated as described in the general procedure. Colorless crystals of **8** were obtained (0.20 g, 16 %). ^{1}H NMR (CD_2Cl_2): δ = 8.61 (d, J = 5.6 Hz, 1H), 8.21 (td, J = 7.8 Hz, J = 1.2 Hz, 1H), 8.12 (d, J = 8.4 Hz, 1H), 7.94 (d, J = 6.8 Hz, 1H), 7.75 (d, J = 7.2 Hz, 1H), 7.40–7.53 ppm (m, 3H); ^{13}C NMR (CD_2Cl_2): δ = 159.2, 149.2–149.3 (m), 147.0–147.1 (m), 144.9, 142.9, 141.0–141.1 (m), 138.7–138.8 (m), 136.2–136.3 (m), 135.7, 132.1, 130.4, 127.5, 123.0, 122.2, 118.9 ppm; ^{19}F NMR (CD_2Cl_2): δ = −133.41 (dd, J_F = 25.2 Hz, J_F = 9.2 Hz, 4F), −159.87 (t, J_F = 20.1 Hz, 2F), −165.16 to −165.29 ppm (m, 4F); ^{11}B NMR (CD_2Cl_2): δ = 0.77; HRMS: *m*/*z* calcd for $C_{23}H_8BF_{10}N$, 499.0590 $[M]^+$; found: 499.0584; elemental analysis calcd (%) for $C_{23}H_8BF_{10}N$: C 55.35, H 1.62, N 2.81; found: C 55.51, H 1.90, N 2.76.

Compound 9: 2-(Benzo[*b*]thiophen-2-yl)pyridine (0.42 g, 2.0 mmol) in THF (50 mL), *n*BuLi (1.6 M in hexane, 1.25 mL, 2.0 mmol), and $BMes_2F$ (0.6 g, 2.0 mmol) were treated as described in the general procedure. Yellow crystals of **9** were obtained (0.56 g, 61 %). ^{1}H NMR (CD_2Cl_2): δ = 8.65 (d, J = 5.6 Hz, 1H), 8.04 (d, J = 7.6 Hz, 1H), 7.98–7.89 (m, 2H), 7.66 (d, J = 8.0 Hz, 1H), 7.35–7.27 (m, 2H), 7.18 (t, J = 6.6 Hz, 1H), 6.68 (s, 4H), 2.18 (s, 6H), 1.90 ppm (s, 12H); ^{13}C NMR (CD_2Cl_2): δ = 155.6,

146.1, 146.0, 141.4, 141.2, 140.3 134.5, 134.1, 130.4, 126.9, 126.2, 125.8, 125.4, 125.0, 123.8, 120.4, 118.5, 24.9, 20.7 ppm; ^{11}B NMR (CD_2Cl_2): $\delta =$ 7.96 ppm; HRMS: *m*/*z* calcd for $C_{31}H_{30}BNS$: 459.2192 $[M]^+$; found: 459.2198; elemental analysis calcd (%) for $C_{31}H_{30}BNS$: C 81.04, H 6.58, N 3.05; found: C 81.68, H 6.81, N 2.99.

Compound 10: 1-(Pyridin-2-yl)-1*H*-indole (0.58 g, 3.0 mmol) in Et_2O (50 mL), LDA (1.8 M in heptane/THF/ethylbenzene, 1.8 mL, 3.2 mmol), and $BMes_2F$ (0.89 g, 3.0 mmol) were reacted by the general procedure. Yellow powder of **10** was obtained (1.10 g, 83 %). ^{1}H NMR (CD_2Cl_2): $\delta =$ 8.23 (d, $J = 6.0$ Hz, 1H), 8.12 (td, $J = 8.0$ Hz, $J = 1.6$ Hz, 1H), 7.87 (d, $J =$ 8.8 Hz, 1H), 7.78 (d, $J = 8.0$ Hz, 1H), 7.49 (dd, $J = 6.6$ Hz, $J = 1.8$ Hz, 1H), 7.28–7.18 (m, 2H), 7.11 (t, $J = 6.6$ Hz, 1H), 6.67 (s, 4H), 6.54 (s, 1H), 2.19 (s, 6H), 1.89 ppm (s, 12H); ^{13}C NMR (CD_2Cl_2): $\delta = 151.2$, 146.1, 143.6, 140.2, 136.8, 134.5, 132.5, 129.9, 122.9, 121.6, 120.8, 117.6, 111.4, 109.8, 105.6, 24.4, 20.7 ppm; ^{11}B NMR (CD_2Cl_2): $\delta = 3.38$ ppm; HRMS: *m*/*z* calcd for $C_{31}H_{31}BN_2$: 442.2580 $[M]^+$; found: 442.2577; elemental analysis calcd (%) for $C_{31}H_{31}BN_2$: C 84.16, H 7.06, N 6.33; found: C 83.21, H 7.22, N 5.65.

Fluorescent quantum yield measurements: Photoluminescence quantum yields of dilute degassed toluene solutions ($A \approx 0.1$) were measured at room temperature using the relative quantum yield method using 9,10-diphenylanthracene as the reference standard ($\Phi = 0.90$).[17]

General procedure used for monitoring photolysis process by ^{1}H NMR spectroscopy: Samples were dissolved in dry C_6D_6 in an NMR tube under inert atmosphere. To remove any traces of oxygen that might be present in the NMR tube, three freeze–pump–thaw cycles were performed using liquid N_2. The photolysis for all compounds except **7** was then performed with either a Rayonet photochemical reactor with irradiation at 350 nm at room temperature or a hand-held UV lamp at 365 nm, followed by recording the ^{1}H NMR spectra after different time periods. For compound **7**, the photolysis was carried out in C_6D_6 with a Spectroline UV lamp at 312 nm.

General procedure used for monitoring photolysis process by UV/Vis spectroscopy: Samples were dissolved in dry degassed toluene in a quartz cuvette ($\approx 10^{-5}$ M), under inert atmosphere in a glove box. After wrapping the cuvette with aluminum foil, it was transferred out and photolysis was then performed using a UVP UVGL-25 Compact UV lamp (365 nm) at room temperature. The UV/Vis spectra were recorded after each exposure time and the exposure times were added up.

DFT calculations: The Gaussian03 program was used for all theoretical calculations, which were carried out at the B3LYP level of theory with 6–311G* as the basis set.[18] For compounds with available X-ray structures, geometric parameters were used as starting points for the geometry optimizations, while the Gaussview software package was used to input starting geometries for compounds without X-ray data.

X-ray diffraction analysis: Single crystals of compounds **2**, **4**, **6**–**9**, and B(7-azaindolyl-2-Br-Py)Mes_2 were obtained from solutions of the compounds in toluene and hexanes. Crystals were mounted on glass fibers and data collection was done on a Bruker Apex II single-crystal X-ray diffractometer, with graphite-monochromated $Mo_{K\alpha}$ radiation operating at 50 kV and 35 mA. Data were processed on a PC using Bruker SHELXTL software package,[19] and corrected for absorption effects. All structures were solved by direct methods. All non-hydrogen atoms were refined anisotropically. The positions of hydrogen atoms were calculated, and their contributions in structural factor calculations were included. Two independent molecules were found in the asymmetric unit of compound **4**. The three methyl groups of the $SiMe_3$ in compound **6** display a rotational disordering with 50 % occupancy for each of the two sites. CCDC-759906 (**2**), -759907 (**4**), -759908 (**6**), -759909 (**7**), -759910 (**8**), -759911 (**9**) and -759912 (B(7-azaindolyl-2-Br-py)Mes_2) contain the supplementary crystallographic data for this paper. These data can be obtained free of charge from The Cambridge Crystallographic Data Centre via www.ccdc.cam.ac.uk/data_request/cif.

Acknowledgements

We thank the Natural Science and Engineering Research Council of Canada for financial support. We are in debt to Dr. Rui-Yao Wang for his assistance in crystal data collections. This work is financially supported by the Natural Sciences and Engineering Research Council of Canada.

[1] a) A. Wakamiya, T. Taniguchi, S. Yamaguchi, *Angew. Chem.* **2006**, *118*, 3242; *Angew. Chem. Int. Ed.* **2006**, *45*, 3170; b) A. Fukazawa, H. Yamada, S. Yamaguchi, *Angew. Chem.* **2008**, *120*, 5664; *Angew. Chem. Int. Ed.* **2008**, *47*, 5582; c) Q. D. Liu, M. S. Mudadu, R. Thummel, Y. Tao, S. Wang, *Adv. Funct. Mater.* **2005**, *15*, 143; d) Y. Cui, S. Wang, *J. Org. Chem.* **2006**, *71*, 6485; e) Y. Cui, Q. D. Liu, D. R. Bai, W. L. Jia, Y. Tao, S. Wang, *Inorg. Chem.* **2005**, *44*, 601; f) S. Wang, *Coord. Chem. Rev.* **2001**, *215*, 79; g) S. F. Liu, Q. Wu, H. L. Schmider, H. Aziz, N. X. Hu, Z. Popović, S. Wang, *J. Am. Chem. Soc.* **2000**, *122*, 3671; h) Q. Wu, M. Esteghamatian, N. X. Hu, Z. Popovic, G. Enright, S. Breeze, S. Wang, *Angew. Chem.* **1999**, *111*, 1039; *Angew. Chem. Int. Ed.* **1999**, *38*, 985; i) Q. Wu, M. Esteghamatian, N. X. Hu, Z. Popovic, G. Enright, S. Wang, Y. Tao, M. D'Iorio, *Chem. Mater.* **2000**, *12*, 79; j) H. Y. Chen, Y. Chi, C. S. Liu, J. K. Yu, Y. M. Cheng, K. S. Chen, P. T. Chou, S. M. Peng, G. H. Lee, A. J. Carty, S. J. Yeh, C. T. Chen, *Adv. Funct. Mater.* **2005**, *15*, 567; k) H. Y. Zhang, C. Huo, K. Q. Ye, P. Zhang, W. J. Tian, Y. Wang, *Inorg. Chem.* **2006**, *45*, 2788; l) Z. L. Zhang, H. Bi, Y. Zhang, D. D. Yao, H. Z. Gao, Y. Fan, H. Y. Zhang, Y. Wang, Y. P. Wang, Z. Y. Chen, D. G. Ma, *Inorg. Chem.* **2009**, *48*, 7230; m) H. Y. Zhang, C. Huo, J. Y. Zhang, P. Zhang, W. J. Tian, Y. Wang, *Chem. Commun.* **2006**, 281.

[2] a) Y. Qin, I. Kiburu, S. Shah, F. Jäkle, *Macromolecules* **2006**, *39*, 9041; b) Y. Qin, I. Kiburu, S. Shah, F. Jäkle, *Org. Lett.* **2006**, *8*, 5227; c) Y. Qin, C. Pagba, P. Piotrowiak, F. Jäkle, *J. Am. Chem. Soc.* **2004**, *126*, 7015; d) T. Iijima, T. Yamamoto, *Macromol. Rapid Commun.* **2004**, *25*, 669; e) A. Meyers, M. Weck, *Macromolecules* **2003**, *36*, 1766; f) T. Yamamoto, I. Yamaguchi, *Polym. Bull.* **2003**, *50*, 55.

[3] a) M. Elbing, G. C. Bazan, *Angew. Chem.* **2008**, *120*, 846; *Angew. Chem. Int. Ed.* **2008**, *47*, 834; b) T. W. Hudnall, C. W. Chiu, F. P. Gabbaï, *Acc. Chem. Res.* **2009**, *42*, 388; c) C. D. Entwistle, T. B. Marder, *Chem. Mater.* **2004**, *16*, 4574; d) G. J. Zhou, C. L. Ho, W. Y. Wong, Q. Wang, D. G. Ma, L. X. Wang, Z. Y. Lin, T. B. Marder, A. Beeby, *Adv. Funct. Mater.* **2008**, *18*, 499; e) F. Jäkle, *Coord. Chem. Rev.* **2006**, *250*, 1107; f) Z. M. Hudson, S. Wang, *Acc. Chem. Res.* **2009**, *42*, 1584; g) Y. Shirota, *J. Mater. Chem.* **2000**, *10*, 1.

[4] a) Y. L. Rao, H. Amarne, S. B. Zhao, T. M. McCormick, S. Martić, Y. Sun, R. Y. Wang, S. Wang, *J. Am. Chem. Soc.* **2008**, *130*, 12898; b) C. Baik, Z. M. Hudson, H. Amarne, S. Wang, *J. Am. Chem. Soc.* **2009**, *131*, 14549.

[5] a) R. Sakamoto, S. Kume, H. Nishihara, *Chem. Eur. J.* **2008**, *14*, 6978; b) S. Kume, H. Nishihara, *Dalton Trans.* **2008**, 3260; c) Y. Yokoyama, M. Saito in *Chiral Photochemistry* (Eds.: Y. Inoue, Y. Ramamurthy), Marcel Dekker, New York, **2004**, Chapter 6, p. 235; d) V. Balzani, A. Credi, M. Venturi, *Molecular Devices and Machines*, Wiley-VCH, Weinheim, **2004**.

[6] a) A. Suzuki, *Acc. Chem. Res.* **1982**, *15*, 178; b) N. Miyaura, A. Suzuki, *Chem. Rev.* **1995**, *95*, 2457.

[7] S. B. Zhao, T. M. McCormick, S. Wang, *Inorg. Chem.* **2007**, *46*, 10965.

[8] B. Wrackmeyer, *Annu. Rep. NMR Spectrosc.* **1988**, *20*, 61.

[9] Y. L. Rao, S. Wang, *Inorg. Chem.* **2009**, *48*, 7698.

[10] a) J. D. Wilkey, G. B. Schuster, *J. Org. Chem.* **1987**, *52*, 2117; b) J. D. Wilkey, G. B. Schuster, *J. Am. Chem. Soc.* **1988**, *110*, 7569.

[11] K. B. Wiberg, *Acc. Chem. Res.* **1996**, *29*, 229.

[12] D. Abdallah, J. Whelan, J. M. Dust, S. Hoz, E. Buncel, *J. Phys. Chem. A* **2009**, *113*, 6640.

[13] A. F. Stange, S. Tokura, M. Kira, *J. Organomet. Chem.* **2000**, *612*, 117.

[14] M. Van den Heuvel, T. A. Van den Berg, R. M. Kellogg, C. T. Choma, B. L. Feringa, *J. Org. Chem.* **2004**, *69*, 250.

[15] a) R. Duchateau, S. J. Lancaster, M. Thornton-Pett, M. Bochmann, *Organometallics* **1997**, *16*, 4995; b) J. Yoshino, N. Kano, T. Kawashima, *Chem. Commun.* **2007**, 559.
[16] R. Köster, P. Binger, *Inorg. Synth.* **1974**, *15*, 149.
[17] a) N. J. Demas, G. A. Crosby, *J. Am. Chem. Soc.* **1970**, *92*, 7262; b) S. Fery-Forgues, D. Lavabre, *J. Chem. Educ.* **1999**, *76*, 1260.
[18] Gaussian 03, Revision C.02, M. J. Frisch, G. W. Trucks, H. B. Schlegel, G. E. Scuseria, M. A. Robb, J. R. Cheeseman, J. A. Montgomery, Jr., T. Vreven, K. N. Kudin, J. C. Burant, J. M. Millam, S. S. Iyengar, J. Tomasi, V. Barone, B. Mennucci, M. Cossi, G. Scalmani, N. Rega, G. A. Petersson, H. Nakatsuji, M. Hada, M. Ehara, K. Toyota, R. Fukuda, J. Hasegawa, M. Ishida, T. Nakajima, Y. Honda, O. Kitao, H. Nakai, M. Klene, X. Li, J. E. Knox, H. P. Hratchian, J. B. Cross, V. Bakken, C. Adamo, J. Jaramillo, R. Gomperts, R. E. Stratmann, O. Yazyev, A. J. Austin, R. Cammi, C. Pomelli, J. W. Ochterski, P. Y. Ayala, K. Morokuma, G. A. Voth, P. Salvador, J. J. Dannenberg, V. G. Zakrzewski, S. Dapprich, A. D. Daniels, M. C. Strain, O. Farkas, D. K. Malick, A. D. Rabuck, K. Raghavachari, J. B. Foresman, J. V. Ortiz, Q. Cui, A. G. Baboul, S. Clifford, J. Cioslowski, B. B. Stefanov, G. Liu, A. Liashenko, P. Piskorz, I. Komaromi, R. L. Martin, D. J. Fox, T. Keith, M. A. Al-Laham, C. Y. Peng, A. Nanayakkara, M. Challacombe, P. M. W. Gill, B. Johnson, W. Chen, M. W. Wong, C. Gonzalez, J. A. Pople, Gaussian, Inc., Wallingford CT, **2004**.
[19] SHELXTL Version 6.14, Bruker AXS, **2000–2003**.

Received: December 30, 2009
Published online: April 8, 2010

